Biosensors and Bioelectronics 252 (2024) 116120

Contents lists available at ScienceDirect

Biosensors and Bioelectronics

journal homepage: www.elsevier.com/locate/bios

Novel high-dense microelectrode array based multimodal bioelectronic monitoring system for cardiac arrhythmia re-entry analysis

Sabine Schmidt [a], Wener Li [c], Mario Schubert [c], Björn Binnewerg [c], Christoph Prönnecke [a], Franziska D. Zitzmann [a], Martin Bulst [d], Sebastian Wegner [d], Matthias Meier [a,b], Kaomei Guan [c], Heinz-Georg Jahnke [a,*]

[a] Centre for Biotechnology and Biomedicine, Biochemical Cell Technology, Leipzig University, Deutscher Platz 5, D-04103, Leipzig, Germany
[b] Helmholtz Pioneer Campus, Helmholtz Zentrum Munich, Neuherberg, Germany
[c] Institute of Pharmacology and Toxicology, Carl Gustav Carus Medical Faculty, Technical University Dresden, Fetscherstraße 74, D-01307, Dresden, Germany
[d] Sciospec Scientific Instruments GmbH, Leipziger Str. 43b, D-04828, Bennewitz, Germany

ARTICLE INFO

Keywords:
Large-area microelectrode array
Rotor pattern detection
Impedimetric contraction strength monitoring
Field potential monitoring
Electrical stimulator-based pacing

ABSTRACT

In recent decades, significant progress has been made in the treatment of heart diseases, particularly in the field of personalized medicine. Despite the development of genetic tests, phenotyping and risk stratification are performed based on clinical findings and invasive *in vivo* techniques, such as stimulation conduction mapping techniques and programmed ventricular pacing. Consequently, label-free non-invasive *in vitro* functional analysis systems are urgently needed for more accurate and effective *in vitro* risk stratification, model-based therapy planning, and clinical safety profile evaluation of drugs. To overcome these limitations, a novel multilayer high-density microelectrode array (HD-MEA), with an optimized configuration of 512 sensing and 4 pacing electrodes on a sensor area of 100 mm^2, was developed for the bioelectronic detection of re-entry arrhythmia patterns. Together with a co-developed front-end, we monitored label-free and in parallel cardiac electrophysiology based on field potential monitoring and mechanical contraction using impedance spectroscopy at the same microelectrode. In proof of principle experiments, human induced pluripotent stem cell (hiPS)-derived cardiomyocytes were cultured on HD-MEAs and used to demonstrate the sensitive quantification of contraction strength modulation by cardioactive drugs such as blebbistatin (IC_{50} = 4.2 μM), omecamtiv and levosimendan. Strikingly, arrhythmia-typical rotor patterns (re-entry) can be induced by optimized electrical stimulation sequences and detected with high spatial resolution. Therefore, we provide a novel cardiac re-entry analysis system as a promising reference point for diagnostic approaches based on *in vitro* assays using patient-specific hiPS-derived cardiomyocytes.

1. Introduction

Human induced pluripotent stem cell-derived cardiomyocytes (hiPS-CMs) have been increasingly recognized as valuable in arrhythmia modeling. As *in vitro* systems, they have the potential to predict drug responses including drug efficacy and toxicity. For all these applications, precise measurement and analysis of the electrical properties of the multicellular syncytium of hiPS-CMs are essential to identify electrophysiological changes, such as the re-entry phenomenon, which is one of the most important causes of lethal cardiac arrhythmias (Tse, 2016). To date, re-entry mechanisms and rotors have only been detected in 2D cell culture systems using optical mapping, after cells were loaded with a voltage-sensitive fluorescent dye (Shinnawi et al., 2019) or transfected with a voltage indicator to detect the change in membrane potential (Shaheen et al., 2018). Both methods have similar limitations. These include dye toxicity, a time delay between voltage changes and changes in the fluorescence signal, a comparatively low signal-to-noise ratio that makes evaluation and especially detection of events with small voltage changes difficult, and a lack of suitability for long-term measurement because of toxicity and/or insufficient stability of the probes. In contrast, microelectrode arrays (MEAs) can overcome these limitations with non-invasive, label-free monitoring in real time: however, the available MEA-Systems so far did not fulfill the challenging requirements for re-entry monitoring.

* Corresponding author.
E-mail address: heinz-georg.jahnke@bbz.uni-leipzig.de (H.-G. Jahnke).

https://doi.org/10.1016/j.bios.2024.116120
Received 31 October 2023; Received in revised form 26 January 2024; Accepted 7 February 2024
Available online 14 February 2024

MEA-based field potential monitoring (FPM) of electrophysiology is widely used in cardiac *in vitro* assays for the punctual analysis of contraction rates and field potential-derived action potential duration. Therefore, only a few microelectrodes (Seidel et al., 2017; Tertoolen et al., 2018) are needed. Approaches for a more comprehensive conduction velocity analysis are limited to the available MEAs with typically 60 microelectrodes (Kussauer et al., 2019), resulting in monitoring area or spatial resolution limitations. Furthermore, high-speed electrochemical impedance spectroscopy (EIS)-based monitoring of mechanical contraction complements the comprehensive analysis of cardiac function. In contrast to FPM, the described EIS-based monitoring systems generally use a single pair of large electrodes (such as interdigital electrodes) (Hu et al., 2018; Wang et al., 2013), which prohibits any spatial resolution. Another technical approach is CMOS-based MEAs with active integrated transistors for field potential amplification and initial on-chip data-stream processing. The major advantage of such CMOS-MEAs is the large number of up to 4096 microelectrodes and more (Emery et al., 2023; Miccoli et al., 2019; Zhao et al., 2023). The disadvantages are the high development and initial set-off fabrication costs, limitation to opaque silicone substrates and amplitude range, and most importantly, limitation to small sensing areas owing to high area-dependent fabrication costs. Therefore, CMOS-MEAs are preferred for the highly-resolved *in vitro* and *in vivo* monitoring of neuronal network activity (Xu et al., 2021). Thus, available MEA systems are not suitable for investigating the more complex electrophysiological phenomena of cardiomyocytes, especially re-entry, because they do not allow the required extension of the monitored cell culture area while maintaining a high spatial resolution. However, this combination is necessary to detect and analyze the rotor patterns. In this context, we aim to fill the gap between the widely used transparent MEAs with a low number of electrodes, which limits the spatial resolution or monitoring area, and CMOS-MEAs, which offer extremely high spatial resolution but are clearly limited in the monitoring area and substrate selection. Moreover, we aimed to develop a MEA-based measurement system capable of comprehensive high-content monitoring of cardiomyocytes, comprising quantitative analysis of electrophysiology and cardiac contraction mechanics with high spatial resolution as well as compatibility with optical monitoring techniques.

2. Materials and methods

2.1. Finite element method (FEM) simulation

FEM simulation was performed using the AC/DC-module of COMSOL Multiphysics 5.4 (Comsol Multiphysics GmbH). Geometries were constructed using COMSOL Multiphysics software. Dielectric properties of the culture medium and chip materials were set as previously described (Jahnke et al., 2019). The simulations were performed using a fully coupled direct solver with the mesh size “fine”.

2.2. Cleanroom fabrication processes

Fabrication of the multilayer HD-MEA was carried out using photolithographic structuring and lift-off processes, as previously described (Schmidt et al., 2022). Briefly, microelectrodes and conducting paths were applied to borosilicate glass substrates by structuring the photoresist AR-N 4340 (Allresist GmbH). A conductive layer of gold (250 nm) was applied via physical vapor deposition (PVD) followed by an SU8-2 passivation layer. Subsequently, the 10 μm interspacer was generated with the SU8 3035 (Kayaku, Ltd.) photoresist. To apply the counter electrodes to the surface of SU8-3035, a novel patterning technique was performed using photoresist AR-P 3510. Counter electrodes and conducting paths were deposited via sputtering. The final structured HD-MEA was bonded to a PCB frame (Multi Circuit Boards, UK) using the conductive adhesive Epo-TEK H20E followed by stabilization with the insulating epoxy resin Epo-Tek ET-302-3M (Epoxy Technology, Germany). For cell cultivation a 35 mm petri dish (Greiner BioOne, Germany) was bonded without the bottom on top of the HD-MEA with biocompatible silicone Loctite 5366 (Henkel GmbH, Germany). Details of all steps are described in the Supplementary Information.

2.3. Bioelectronic measurement system

For the initial multimodal evaluation experiments a self-developed hybrid front-end was combined with a specifically adapted MSX-8 data acquisition (DAQ) system obtained from Sciospec Scientific Instruments GmbH. Briefly, the system comprised four 96 channel amplifier (200x) data acquisition modules and four high-precision impedance spectroscopy modules. For automated measurements, LabView (National Instruments)-based programs were developed for impedance measurements (IMATadvanced) and field potential monitoring (FiPRAT). Impedance spectra were recorded from 500 Hz to 5 MHz (51 frequency points) and a signal amplitude of ± 10 mV. Field potential streams were recorded at a sampling rate of 4 kHz. To monitor all 512 microelectrodes in parallel, a specifically designed, highly integrated measurement-system was developed by Sciospec Scientific Instruments GmbH. It allows fully simultaneous measurement on 512 channels, high acquisition rates of up to 50 kHz, and flexible channel function assignments (field potential amplifier and impedance analyzer). For low noise and minimum cable complexity the entire measurement section of the system can be placed into a cell incubator. The measurement system control and data recording were realized using the self-developed program FiPRAT.

2.4. Cell culture

Culturing of the human induced pluripotent stem (hiPS) cell line IMR90C01 (WiCell Stem Cell bBank, USA) and differentiation into human atrial cardiomyocytes (hiPS-aCMs) was performed as previously described (Fleischer et al., 2019). Briefly, differentiation was initiated with 1 μM CHIR98014 (Santa Cruz Biotechnology, Germany), followed by medium exchange after 24 h without CHIR98014 and addition of 1 μM IWP-4 (Miltenyi Biotec, Germany) for 48 h. First spontaneous contractions were observed within 8–12 days. Beating cardiomyocyte cultures were dissociated on day 23 with 0.25 % trypsin-EDTA (ThermoFischer, Germany) and 0.5 mg/mL DNase I (AppliChem, Germany) for 30 min at 37 °C followed by mechanical separation. After centrifugation at 500×*g* for 5 min, the cells were reseeded on Matrigel (Corning, Germany)-coated (diluted 1:50) HD-MEA.

A previously characterized hiPS cell line, iBM76.3, generated from a healthy donor was subtype-specifically differentiated into hiPS-aCMs (Cyganek et al., 2018). On day 15, the hiPS-aCMs were replaced and further cultured in a custom-modified maturation medium (Feyen et al., 2020). On approximately day 78, hiPS-aCMs were digested and seeded onto the HD-MEA. hiPS-aCMs were cultured in maturation medium for an additional 7 days to recover from digestion before being used for FPM based analysis. For all hiPS derived cardiomyocytes 1.5 million cells were seeded per HD-MEA.

Atrial-derived cardiac cell line HL-1 was cultured in culture flasks or on HD-MEA, coated with gelatine/fibronectin for 24 h, using Claycomb medium (Sigma-Aldrich, Germany) supplemented with 10 % fetal bovine serum (ThermoFischer, Germany), 2 mM GlutaMAX™ (ThermoFischer, Germany) and 0.1 mM norepinephrine (Sigma-Aldrich, Germany). HL-1 cell cultures were maintained at 37 °C in a humidified atmosphere with 5 % CO_2. 1 million HL-1 cells were cultured on gelatine/fibronectin coated HD-MEA till the state of 100 % confluence and synchronous contraction.

2.5. Data analysis and statistics

Field potential data streams were recorded and processed for analysis using the LabView-based self-developed program FiPRAT. To

statistically analyze the contraction rate and action potential amplitude, a dynamic threshold-based peak-detection algorithm was used to continuously determine the noise-level of each microelectrode data stream using median analysis, as previously described (Quiroga et al., 2004) and a factor of six to obtain the absolute threshold level. The algorithm for the advanced analysis of conduction transmission by magnitude and phase mapping includes several processing steps, as described in the results section. The algorithm was integrated into the LabView module for integration into the FiPRAT program. The magnitude and phase maps shown are the averages of three frames. Highly time-resolved impedimetric time traces for contraction monitoring were processed and analyzed using the EIS recording program IMA-Tadvanced. Impedance spectra data was analyzed using the self-developed LabView based software IDAT v4, which calculates the cellular contribution from the impedance magnitude spectra ($(|Z|_{cell} - |Z|_{cell\text{-}free})/|Z|_{cell\text{-}free} \times 100\%$) and determines the maximum value for each spectrum. The recorded field potential streams were analyzed using a self-developed software (FiPRAT, LabView). GraphPad Prism 9 (GraphPad Software, San Diego, CA, USA) was used for all statistical analyses. Multiple group comparisons for significant effects were performed using repeated 2D-ANOVA test with Tukey's post-hoc test (recommended by GraphPad Prism).

3. Results and discussion

3.1. Design and fabrication of high-density microelectrode array

The challenge in detecting and tracing complex stimulus conduction patterns is to cover a sufficient sensing area with appropriate resolution. Regarding the use of passive microelectrode based monitoring, our aim was to increase the number of microelectrodes beyond the typical number of approximately 60 (Seidel et al., 2017; Tertoolen et al., 2018) in more advanced systems with 256 microelectrodes to cover an area of approximately 100 mm^2. In this context, the critical limitation is not only given by the number of data acquisition (DAQ) channels for low-noise parallel recording, but also the number and length of conducting paths as well as the robust contacting with the DAQ-system. Because conducting paths require a certain width and interspace with regard to the fabrication and crosstalk, we started with a FEM simulation to analyze the influence of the conducting path interspace on the field potential crosstalk (Fig. S1A). The simulation results revealed no critical crosstalk (10^{-8}-10^{-7} µV) down to an interspace of 5 µm (Fig. S1B). Next, we fabricated test micro-arrays with conducting path interspaces in the range of 7.5 µm–50 µm to evaluate this via experiments (Figs. S1C and D). While for conducting paths interspaces down to 15 µm no obvious crosstalk was observed, an interspace of 7.5 µm led to more frequent occurrence of distinct crosstalk between neighboring conducting paths (Fig. S1E). As the FEM-simulation revealed no such high crosstalk in the range of 10–100 µV, and this high crosstalk only occurred sporadically, we attributed this to fabrication limitations, such as hairline-like residual structures causing near shorts. Therefore, we defined the design rules of minimum 15 µm conducting path interspacing as well as conducting path width. Based on these rules, including the monitoring area with the highest possible density and contacting and DAQ-channel limitations, the design approaches led to a number of 512 microelectrodes. Although this could be realized with the highest possible density within one plane, the integration of the reference and counter electrodes of an appropriate size for FPM and EIS could not be realized in the same plane. The only solution to this problem is a multilayer design (Fig. 1A) with an SU8 insulation layer between the two conductive planes. To ensure reliable

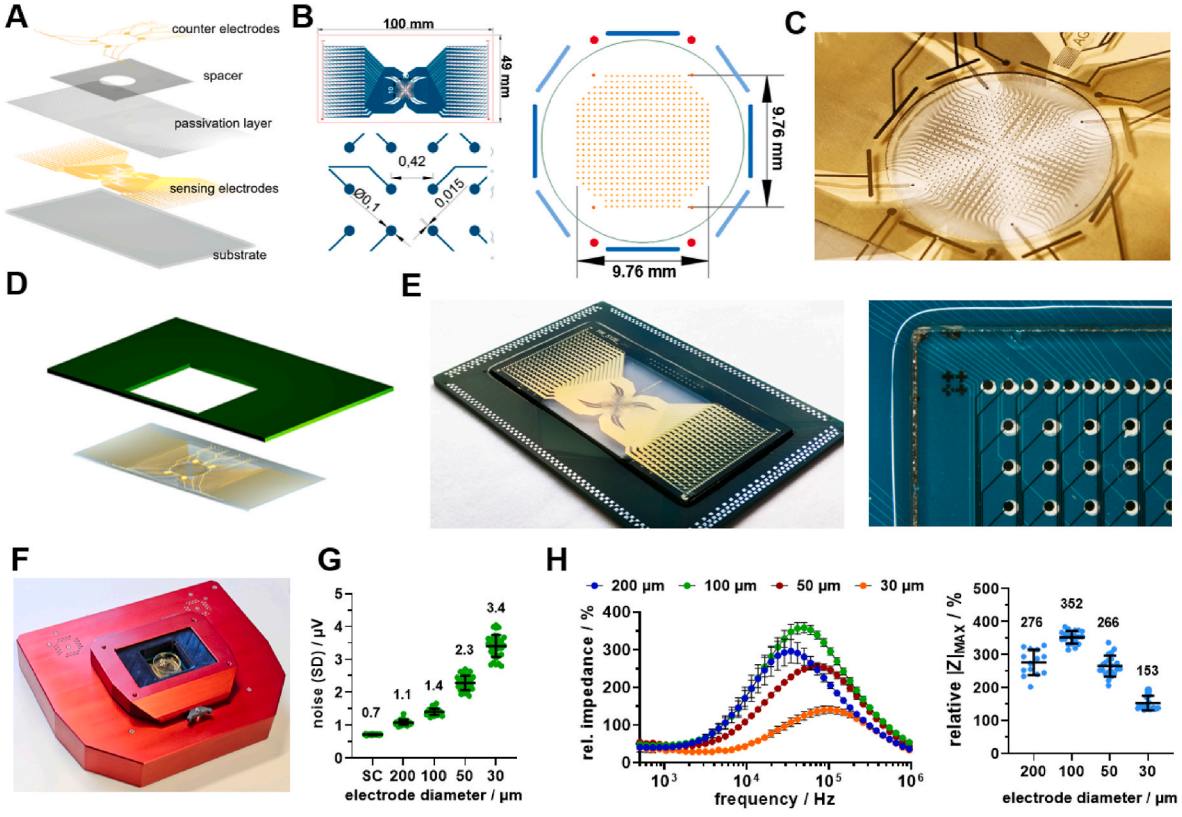

Fig. 1. Description of high-dense microelectrode array (HD-MEA) and electrochemical characterization. (A) Schematic view of the multi-layered structure with (B) dimensions of microelectrode array and circuit paths. (C) Image of the fabricated HD-MEA scheme and photo of whole measurement setup. (D) Scheme of connection PCB with (E) images of the bonded structured HD-MEA to the PCB. (F) 384-channel hybrid-measurement system for initial characterization of (G) electrode size dependent as well as short circuit (SC) basic noise of field potential signals (n = 36, mean ± sd) and (H) relative impedance spectra representing the impedimetric cell signal (n = 4, mean ± sd) with an analysis of the maximum relative impedance/cell signal (n = 36, mean ± sd).

electrical isolation and define a cultivation area, an SU8 interspacer with a thickness of 10 μm was included. The final design (Fig. 1B, Fig. S2) comprised the first plane on a 100 mm × 49 mm glass substrate for all conducting paths and contacting points as well as 512 microelectrodes at a distance of 420 μm from each other, resulting in a monitoring area of approximately 100 mm^2 (95.3 mm^2). After several fabrication process optimizations, especially regarding the multilayer adhesion and durability, the HD-MEA was successfully fabricated (Fig. 1C). Next, contacting to the measurement system had to be realized. Therefore, a printed circuit board (PCB) frame, (Fig. 1D), which can be easily adapted to different front-end systems, was used. The PCB frame was designed according to the ANSI/SLAS 2–2004 footprint dimensions for microtiter plates (127.76 mm × 85.48 mm) as well as the position of the well B2 of a 6-well microtiter plate for the monitoring/cultivation area. Although our HD-MEA based system is not focused on high-throughput applications, the laborious cultivation and culture maintenance before experiments take place are often a bottleneck in real world applications. In this context, a high number of HD-MEAs can be easily stacked and handled in parallel like microtiter plates or even processed by automated/robotic cultivation and maintenance systems for microtiter plates.

For the initial evaluation, we designed a PCB-adapter that matched a self-developed 384 channel hybrid FPM and EIS measurement system based on a MSX8-DAQ system. Robust and reliable bonding of the glass substrate to the PCB was achieved using highly conductive glue at the contact points and was stabilized using epoxy resin bonding in the interspaces (Fig. 1E). Thus, the HD-MEA was easily contacted using the self-developed front-end (Fig. 1F, Fig. S3) in combination with the MSX8-DAQ system, provides the possibility of application to the FPM and high-precision EIS on the same microelectrode.

Next, we evaluated the optimal electrode size with respect to basic noise level (FPM), self-impedance, and achievable cell signal. Therefore, microelectrode diameters of 30–200 μm were analyzed. First, the basic noise-level of the field potential amplifier DAQ-channels were determined using a short-circuit PCB (SC), which revealed 0.7 μV (Fig. 1G). The analysis of the electrode diameter showed increasing noise with smaller diameters, especially for diameters smaller than 100 μm. Second, we recorded the impedance spectra for each electrode size (Fig. S4), showing a typical size-dependent increase in the self-impedance with a smaller electrode size (Schmidt et al., 2022). No further deviations were observed, which proved the high quality of the glued connections and the absence of distinct crosstalk between the conducting paths. Afterwards, we cultivated HL-1 cells on the microelectrodes up to confluence, and determined the achievable cell signals reflected by the relative impedance spectra (Fig. 1H). The relative impedance spectra showed distinct cell signals in the range of 10–500 kHz with an electrode diameter dependent maximum signal and frequency, where it occurs.

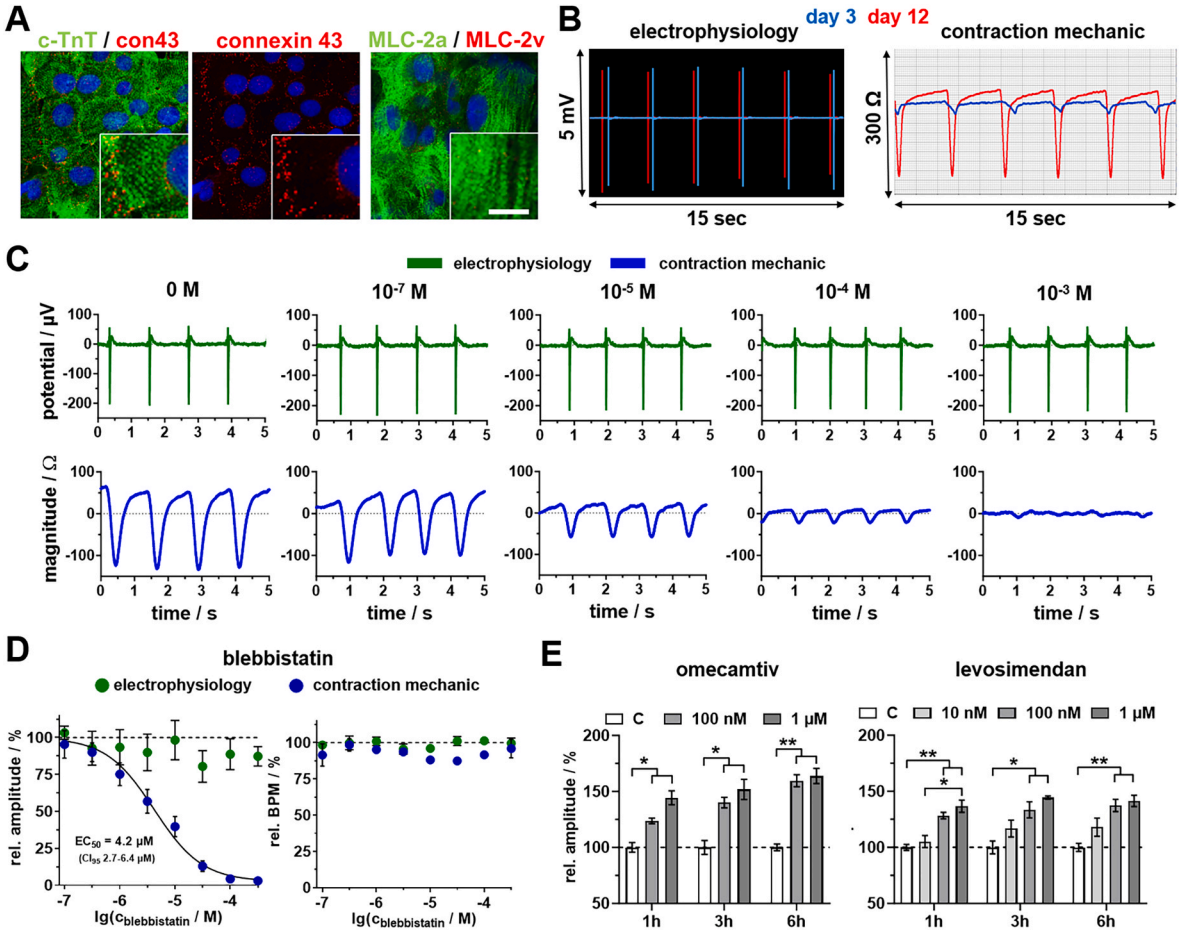

Fig. 2. Multimodal monitoring of human induced pluripotent stem cell (hiPS)-derived cardiomyocyte cultures. (A) Immunocytochemical characterization of hiPS derived cardiomyocyte cultures after 35 days of differentiation (represents 12 days cultured on HD-MEA) with cardiac markers (red/green) and DAPI nuclei stain (blue) (scale bar: 25 μm, for insert 10 μm). (B) Representative field potential signals for action potential characterization and contraction strength using highly time-resolved impedimetric monitoring. (C) Representative FPM and impedance signal time traces for different concentrations of the myosin II (contraction) inhibitor blebbistatin, which causes electro-motoric-decoupling (EMD) in contracting cardiomyocytes. (D) Contraction rate in beats per minute (BPM) and signal amplitude determined by field potential monitoring (electrophysiology) and impedimetric monitoring (contraction strength) for the quantitative analysis of the blebbistatin effect (n = 4, mean ± sem). (E) Impedimetric analysis of time dependent effect of Ca^{2+} sensitizer therapeutics on contraction strength (n = 4, mean ± sem, *p < 0.05, **p < 0.01).

The statistical analysis of the maximum achievable cell signal revealed the highest values for an electrode diameter of 100 μm and notably lower values for bigger and smaller electrodes. Based on this result and with respect to the FPM basic noise, an optimum electrode diameter of 100 μm was selected for all further HD-MEA fabrication (Fig. 1B).

3.2. Microelectrode based multimodal monitoring of electrophysiology and cardiomyocyte contraction strength

Based on the fabricated HD-MEA, the capabilities of the microelectrode based multimodal monitoring of cardiomyocytes should be demonstrated. Therefore, hiPS-aCMs were cultured on HD-MEAs, resulting in functional syncytial cultures with spontaneous contractions after 2–3 days. The atrial subtype (MLC-2a), as well as a high degree of cell-cell connections by gap-junctions (connexin 43) were confirmed by immunocytochemical staining (Fig. 2A). In the first step, FPM was used to analyze the cardiac electrophysiology within the first two weeks after seeding and high time-resolved impedance spectroscopy was applied to monitor the contraction strength of cardiomyocytes. Based on the capabilities of the high-precision impedance analyzer modules within the MSX-8 DAQ-system, a sampling rate of 500 samples/s was achieved at a single frequency of 50 kHz (highest cell signal), which allowed the detection of the mechanical contraction of cardiomyocytes at a high temporal resolution (Fig. S5). Although this has been previously described for large-area electrodes (Hu et al., 2018; Wang et al., 2013), to the best of our knowledge this has not been demonstrated for microelectrodes before, which may be due to the fact that the high intrinsic impedance of microelectrodes in the 10^4–10^5 Ω range (Fig. S5A) requires a measurement system with sufficient precision at such high impedances as well as temporal resolution. To ensure the formation of a dense cardiomyocyte cell layer as a prerequisite for reproducible functional analysis, we monitored relative impedance spectra (cellular contribution), which revealed reproducible homogenous dense cell layers after 7 days (Fig. S6A). In addition, reusability of HD-MEAs as well as viability of the established cardiomyocyte cell layer could be proved (Figs. S6B and C). Based on this, the use of our self-developed system in combination with the HD-MEA allowed the monitoring of cardiac electrophysiology and contraction strength on the same microelectrode for 384 microelectrodes in parallel (Fig. S7). Monitoring within the first 12 days after seeding revealed strong and robust electrophysiology with high amplitude action potentials after 2–3 days (Fig. 2B) and in contrast, only weak contraction mechanic related impedance signal amplitudes within the first 5 days. Subsequently, the impedance signal amplitudes clearly increased, which was in line with the microscopic observations (Suppl. Mov. 1). To prove the correlation of mechanic contraction and periodic alterations of impedance magnitude, we acquired microscopic images and impedance magnitude in parallel for a time-synchronized overlay (Suppl. Mov. 2). Additionally, hiPS derived atrial cardiomyocytes were cultivated for 70 days on HD-MEAs to investigate long-term stability (Fig. S8). A high level of electrophysiological activity and contraction functionality was observed over the entire time period (Fig. S8A). In correlation, the monitoring of cell layer density and homogeneity based on relative impedance spectra showed a rather dense layer over the whole period (no spectra with maximum values around zero) with a more heterogeneous distribution especially after 70 days (Fig. S8B). The microscopic analysis of live-dead staining after 70 days (Fig. S8C) revealed a quite dense and viable cell-layer but with a distinct cell clustering and dome formation on the surface, which correlates with the higher variance of relative impedance spectra at this time point. Taken together these results demonstrates the reproducibility, long-term stability, and suitability of our HD-MEA based measurement setup to comprehensively characterize cardiac functionality.

Based on this capability, we analyzed the effects of compounds and therapeutics on electro-motoric-coupling. First, we applied the myosin-2 ATPase inhibitor blebbistatin (Kovacs et al., 2004) in an ascending concentration and accumulative scheme to four different HD-MEAs in hiPS-derived cardiomyocyte cultures. The monitoring revealed a clear concentration-dependent decrease in the contraction strength (EIS derived amplitude) with no distinct effect on the electrophysiology (Fig. 2C). The statistical concentration-response analysis from four experiments revealed an IC_{50} value of 4.2 μM (Fig. 2D), which is in line with the reported values in the range of 0.5–5 μM (Limouze et al., 2004). In contrast, the FPM revealed no distinct decrease in the field potential amplitude. Additionally, the highly resolved impedimetric traces allowed the detection of residual contractions, although the signal was attenuated by more than 90 % for blebbistatin concentrations higher than 30 μM (Fig. 2C). Thus, contraction rates were determined using FPM and EIS, and neither showed any distinct alterations. This shows the specific effect of blebbistatin on the contraction mechanics without influencing the electrophysiology of the functional cardiac syncytium, and clearly demonstrates the capabilities of our HD-MEA-based measurement system to quantitatively monitor such effects. In the next step, we analyzed the effect of the experimental therapeutics omecamtiv (Fig. S9, Fig. 2E), a myosin activator leading to increased contraction strength (Nagy et al., 2015), as well as levosimendan (Fig. 2E), a calcium sensitizer that binds to cardiac troponin-C and leads to an increased contraction strength (Kaheinen et al., 2006). We monitored the effects of both compounds over a time range of 6 h at different concentrations, with four independent samples (MEAs) for each concentration. A comparison of the contraction strength related impedance signal amplitudes revealed a significant increase for both compounds in concentration- and time-dependent manners. More strikingly, these results are in line with literature values for omecamtiv (maximum effect in the range of 0.3–1 μM) (Nagy et al., 2015) and levosimendan, with a maximum strengthening effect on primary human cardiomyocyte strips at 0.8 μM (Hasenfuss et al., 1998). To the best of our knowledge, this is the first description for an EIS based quantitative monitoring of contraction strengthening effects of therapeutics such as omecamtiv and levosimendan, using a hiPS derived cardiomyocyte *in vitro* culture model.

3.3. HD-MEA based detection of rotor patterns

Based on the encouraging demonstration of the HD-MEA capabilities for sensitive multimodal monitoring, we realized a comprehensive measurement system with DAQ-channels for all 512 microelectrodes that can be operated under standard cell culture conditions (37 °C, 5 % CO_2, 95 % humidity) and finally, allows the detection and analysis of complex stimulus conduction patterns. In this context, a customized, compact measurement system was developed with 512 independent parallel DAQ-channels in a cell culture incubator compatible front-end (Fig. 3A) that is connected to a MS Windows-based X86 computer via USB 2.0. Using the high-speed data transfer mode, the system could be reliably operated at a 20 kHz sampling rate for all 512 channels in parallel (22 MB/s) over days. Sampling rates of 40 kHz were also achieved, although sporadic data stream interruptions were observed due to the performance limitations of the MS Windows based-computer system. For an easy and robust contact of more than 520 contacts, alternatives to the commonly used contact spring pins were examined with regard to the contact number, space, and contact pressure requirements. With low profile interconnectors from SAMTEC that comprise an array of up to 300 micro springs on both sides (Fig. 3A) a suitable solution was found. Thus, two interconnected arrays are sufficient. Based on an adapted PCB-frame HD-MEAs can be easily connected to the front-end with a simple metal bracket and three screws (Fig. 3A). The initial characterization of the basic field potential amplifier noise (100 μm microelectrode diameter) revealed an excellent noise level of 1.2 μV. Next, the cardiac HL-1 cell line (Fig. 3B) was used for the initial functional test. HL-1 cells are of murine origin and is the only known immortalized cell line that shows functional electrophysiology and mechanical contraction in confluent 2D cultures (Claycomb et al., 1998). Therefore, the HL-1 cells were highly suitable for testing function of the HD-MEA in

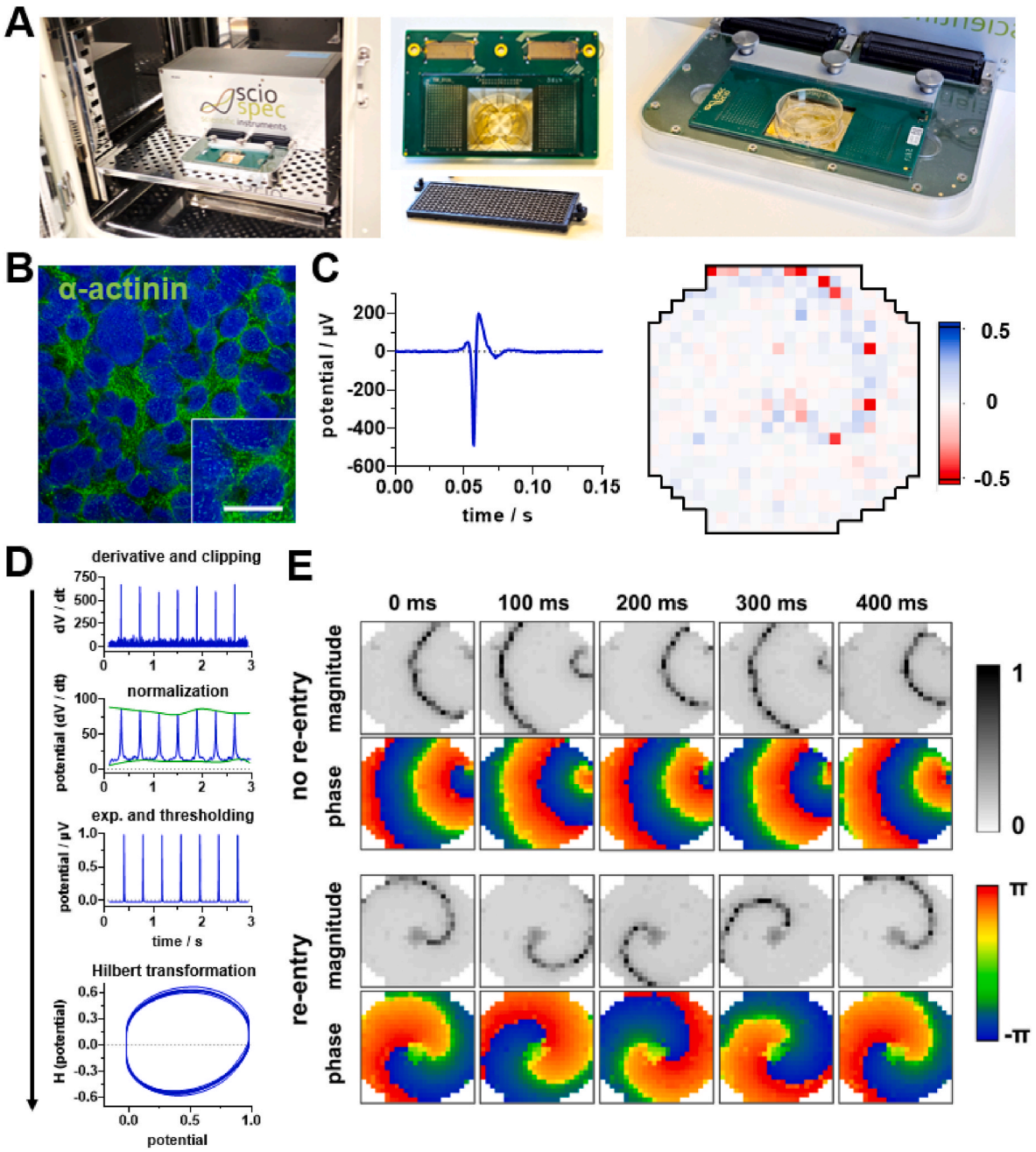

Fig. 3. HD-MEA based detection of rotor patterns. (A) Integrated monitoring system within a cell incubator and adapted connecting PCB. To realize more than 530 interconnects, two interconnectors with 300 micro-springs on both sides are used that allow an easy connection of the HD-MEA with a metal bar and three screws on the DAQ-system. (B) Immunocytochemical staining of cardiac α-actinin on confluent HL-1 cell culture and DAPI nuclei stain (blue) (scale bar: 20 µm, for insert 10 µm). (C) Exemplarily HL-1 cardiomyocyte derived field potential of one single electrode (left) and spatial resolved sample of normalized potential based on all 512 microelectrodes (right). (D) Main steps of field potential data stream processing pipeline with final phase calculation by Hilbert transformation. (E) The result of data processing are normalized magnitude and phase signal traces, which revealed spontaneous re-entry events visualized by the rotor pattern.

combination with the 512-channel measurement system. Using HD-MEAs with a confluent functional syncytium and optically visible contraction, action potentials with amplitudes of up to 1 mV were observed (Fig. 3C). Based on the spatial resolution obtained using signals from all 512 microelectrodes (Fig. S10), the stimulation conduction pattern was clearly visualized (Fig. 3C, right). For automatic action potential detection and further data processing regarding re-entry-related rotor pattern detection and visualization, a complex data processing pipeline was established (Fig. 3D) based on a previous work for electrogram data derived from *in vivo* recordings (Roney et al., 2017). In detail, field potential data streams were low-pass filtered (100 Hz) followed by forming the first derivative, clipping of all positive values and negation of all values. Afterwards, the data stream was again low-pass filtered (10 Hz) and normalized with regards to the peak heights and baseline signal trace. Next, the signal trace was raised to a power of six and truncated at one to dampen low-amplitude nonspecific deflections that could disturb the computation of the phase angles. Finally, the phase angles were calculated using Hilbert transformation, resulting in normalized magnitude and phase maps for each recorded time point (sample). Although most of the analyzed HL-1 cultures showed the expected linear conduction transmission profile from a randomly located pacemaker center, some individual HL-1 cultures

showed spontaneous rotor patterns (Fig. 3E). As this is usually only observed after the application of arrhythmia-causing drugs or pacing (Shinnawi et al., 2019), it was unexpected. However, as atrial-like murine HL-1 cells are an artificially immortalized and degenerated cell line, this may be an explanation for the spontaneous occurrence of arrhythmia-related re-entry patterns.

Regardless, the observed rotor patterns successfully demonstrate the capability of our developed large-area HD-MEA, in combination with the novel 512 channel measurement system to detect and map such patterns.

3.4. *Integrated multipoint stimulation allows cardiomyocyte pacing and re-entry induction*

After successful demonstration of monitoring re-entry-caused rotor patterns, we focused at the more clinically and diagnostically relevant hiPS-CM culture model. As expected, no spontaneous occurring rotor patterns were observed. Although induction can be achieved by arrhythmia-causing drugs, this could be critical in future with respect to therapeutics testing against arrhythmia. Instead, we aimed to develop a more versatile and robust method based on the *in vivo* condition of patients, where stress and overstimulation induce re-entry (Cluitmans et al., 2023). Therefore, electrical stimulation is an appropriate way to induce re-entry patterns (Shaheen et al., 2018). Most electrical stimulation systems for cardiac pacing are based on external units with commercially obtained or self-fabricated large area plate or rod electrodes (Hirt et al., 2014; Shaheen et al., 2018; Stoppel et al., 2016) and are introduced from the top of the culture, for example in a modified lid. This has the advantage of strong fields over a large area while maintaining a safe distance from the injected current to prevent potential cell damage. However, this requires a manual positioning step from the top and is less accurate with regard to positioning and distance, as well as offers limited application of specific spatial stimulation patterns owing to the large electrodes and the resulting field-covering area. To overcome these limitations, we integrated stimulation electrodes directly onto the four edges of the microelectrode array. As the available space is clearly limited, the needed stimulus electrode area was evaluated with the help of a multielectrode array comprising electrode areas of 0.8–5 mm^2 for a reliable pacing of hiPS-CM cultures. The evaluation revealed a minimum of at least 2.5 mm^2–4 mm^2 for being able to reproducibly pace cardiomyocytes with bipolar 1 ms pulses of ±1 V to ±2 V (Suppl. Mov. 3). Based on these results, an adapted design was created with four integrated stimulation electrodes (4.5 mm^2) and larger counter electrodes for bipolar stimulation (Fig. 4A). To drive the stimulator electrodes, four independent stimulation modules were integrated into a 512-channel DAQ-system. Thus, hiPS-CMs with a slow beating frequency (<10 bpm) were used to evaluate the adapted HD-MEA (Fig. 4B). Although ±1 V pulses with 2 ms pulse duration, were not able to pace the hiPS-CMs with each pulse at 1 Hz, amplitudes of ±1.5 V (Suppl. Mov. 4) and greater led to reliable pacing, even at a pulse frequency of 2 Hz. The successful coupling was proven by FPM and microscopic monitoring.

Finally, we attempted to induce re-entry into hiPS-derived atrial cardiomyocytes (aCMs) cultured on HD-MEA using our integrated stimulation module. Different pacing frequencies (4, 6, 8, 10 and 20 Hz) with different bipolar pulses (±2–5 V, 2–2.5 ms pulse duration) were tested. We found that 85-day-old hiPS-derived cardiomyocytes from a healthy donor showed extremely low susceptibility to re-entry induction. Induction of re-entry could only be achieved at higher pacing frequencies, whereas lower pacing frequencies (less than 8 Hz) could not induce any re-entry in 85-day-old hiPS-derived cardiomyocytes aquired from a healthy donor. Fig. 5A shows a stimulation protocol with 30 bipolar pulses (±5 V, 2.5 ms pulse duration) at a frequency of 20 Hz. This burst pacing led to successful transient re-entry induction in an 85-day-old hiPS-derived cardiomyocyte culture (Fig. 5A), as demonstrated by magnitude and phase mapping (Fig. 5B) established for HL-1 cardiomyocyte data streams (see Fig. 3). Magnitude and phase analyses showed that the induced re-entry pattern lasted for 4 s and then returned to a regular rhythm prior to pacing (Fig. 5B). Thus, proof of the functional pacing of human cardiomyocytes could be provided, and more strikingly, arrhythmia-related re-entry events could be induced by the

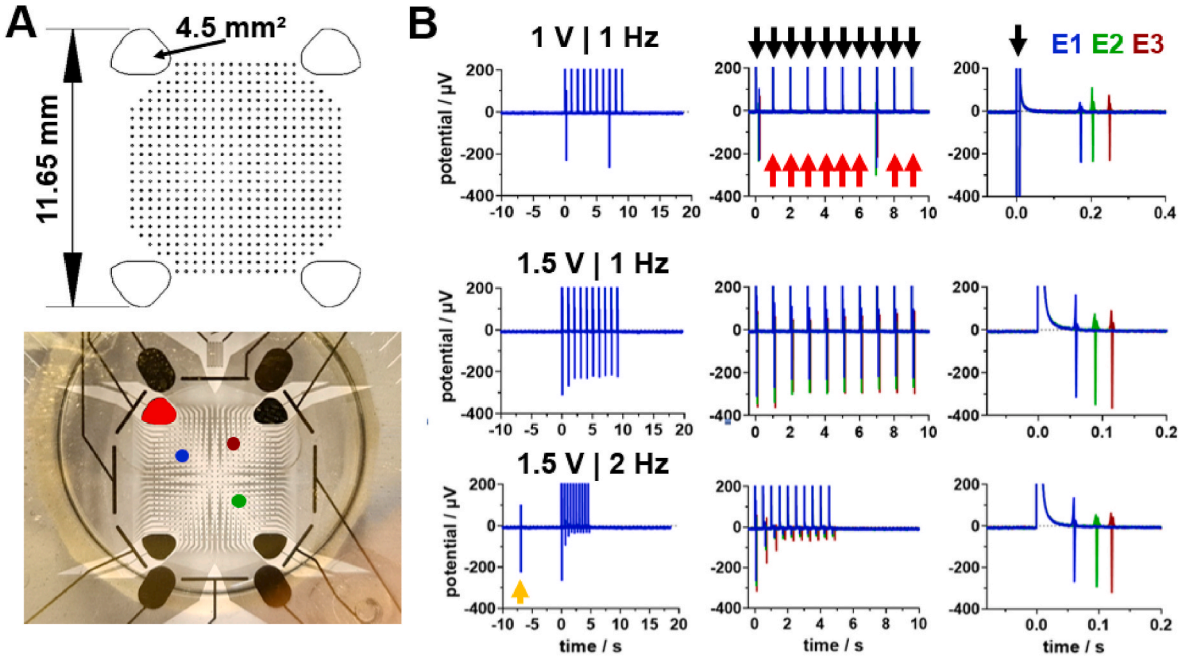

Fig. 4. Integration of multipoint stimulation electrodes for cardiomyocyte pacing. (A) Scheme and image of adapted HD-MEA with a stimulation electrode in each corner of the cultivation area and four counter electrodes for bipolar stimulation. In the image, colored marks represent monitoring (E1-E3) and stimulation (red) electrodes. (B) Field potential traces of three electrodes (E1-E3) from a hiPS-CM culture paced with 10 bipolar pulses (±1V or 1.5V, duration 1 ms) at 1 Hz or 2 Hz. Black, red, and orange arrows mark stimulation artefacts (not marked in 30 s time trace), missing action potentials (no stimulation), spontaneous action potential, respectively.

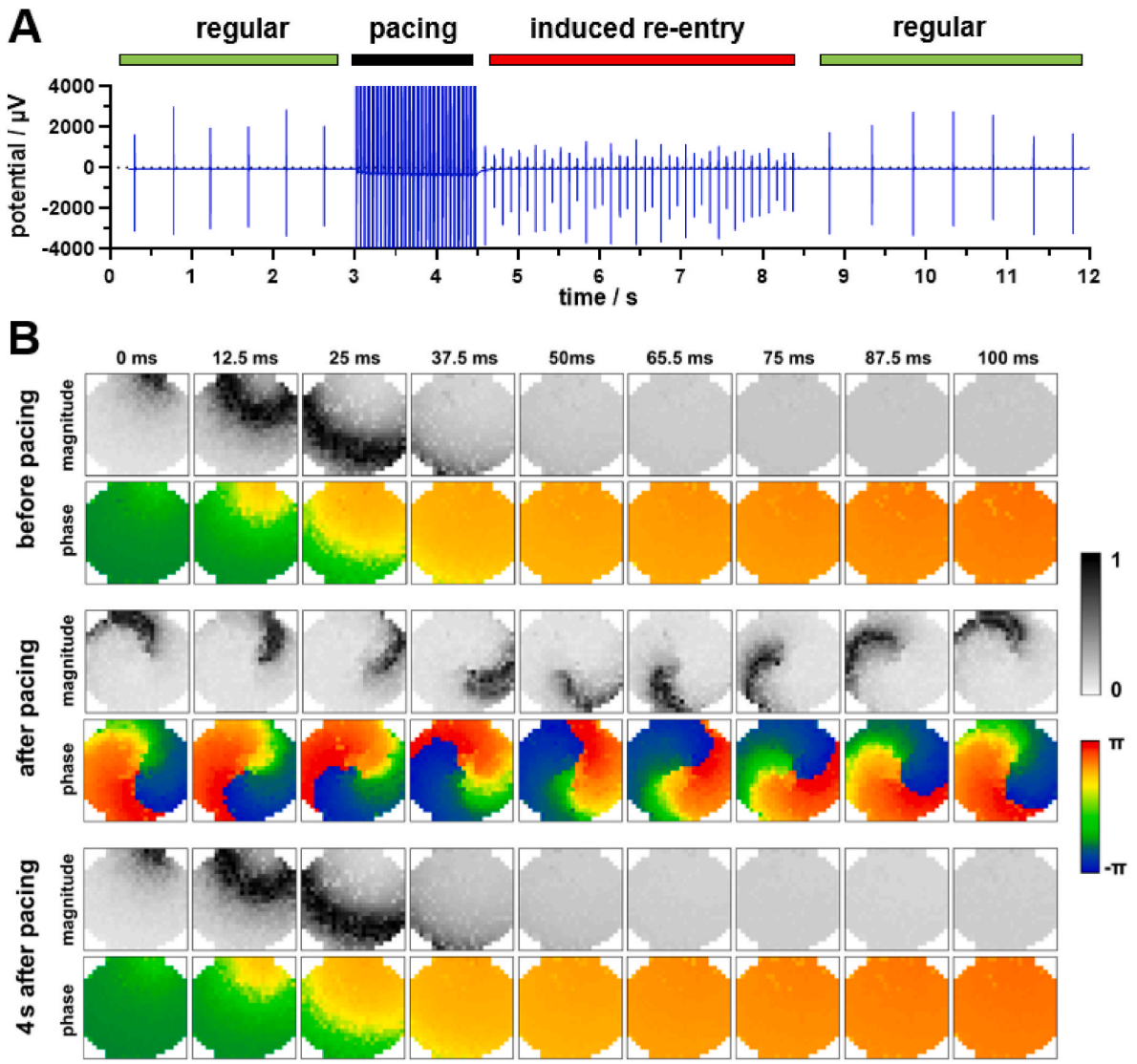

Fig. 5. Electrical stimulator induced transient re-entry in hiPS-aCMs. (A) Exemplarily shown field potential trace (one randomly selected electrode from 512 electrodes) from a spontaneous contracting (regular) hiPS-derived cardiomyocyte culture that was paced with 30 bipolar pulses (20 Hz with ± 5 V, 2.5 ms pulse duration) and (B) the full data stream derived normalized magnitude and phase maps before and direct after pacing as well as 4 s after pacing, which reveals the transient induction of rotor pattern (re-entry).

integrated stimulation system. In the future, using the established burst pacing protocol with increasing pacing frequencies, we can determine the susceptibility of hiPS-derived cardiomyocytes from patients with arrhythmia diseases to re-entry induction and test anti-arrhythmic drugs. The established data processing based on the HD-MEA with 512 microelectrodes enables the comparison of rotor pattern visualization. Consequently, the analyses based on this approach can be compared to the fluorescence dye based optical analyses (Pandit and Jalife, 2013; Shaheen et al., 2018). In addition, both the optically highly transparent HD-MEA and the front-end are compatible with microscope systems (Suppl. Mov. 2), and thus can be used in combination with established state-of-art analyses/assays (e.g. calcium imaging, dye-based voltage sensing).

4. Conclusion

In the presented study, we were able to demonstrate the successful development and application of a large-area high-dense microelectrode array, which fills the gap between available low electrode number MEAs with low spatial resolution and high electrode number CMOS-MEAs with limited monitoring areas (Table S2). Using classical lift-off structuring techniques and a multilayer approach an array with 512 microelectrodes covering an area of approximately 100 mm^2 and all conducting paths and contacts were realized. To the best of our knowledge, this is the first microelectrode array-based comprehensive high-content functional analysis of cardiac electrophysiology and contractility mechanics in. Moreover, the successful induction of re-entry patterns by the integrated multipoint electrical stimulation system, as well as the highly time-resolved (4 kHz) detection and tracing of re-entry-caused rotor patterns now offers a suitable alternative to artificial fluorescence label based microscopic detection techniques for re-entry analysis. Although the resolution with 512 microelectrode cannot compete with microscopical resolution, the advantages of label-free and non-invasive monitoring paves the way for clinically relevant *in vitro* applications such as drug safety testing, development of model-based diagnostics (Chang et al., 2009), and therapy planning (Azzolin et al., 2021). Therefore, the next step will be the application of our developed HD-MEA-based monitoring system to systematically analyze hiPS-derived cardiomyocyte cultures of patients with arrhythmia versus control cultures with regard to re-entry induction susceptibility,

duration, rotation frequency and more advanced re-entry-related parameters (Azzolin et al., 2021; Shinnawi et al., 2019), as well as the effect of antiarrhythmic therapeutics to attenuate or inhibit re-entry-induced patterns (Azzolin et al., 2021).

CRediT authorship contribution statement

Sabine Schmidt: Conceptualization, Investigation, Visualization, Writing – original draft. **Wener Li:** Investigation, Methodology, Writing – review & editing. **Mario Schubert:** Conceptualization, Methodology, Writing – review & editing. **Björn Binnewerg:** Data curation, Methodology, Software, Writing – review & editing. **Christoph Prönnecke:** Investigation, Methodology. **Franziska D. Zitzmann:** Methodology, Writing – original draft, Writing – review & editing. **Martin Bulst:** Conceptualization, Methodology, Writing – review & editing. **Sebastian Wegner:** Conceptualization, Methodology, Supervision, Writing – review & editing. **Matthias Meier:** Conceptualization, Resources, Writing – review & editing. **Kaomei Guan:** Conceptualization, Funding acquisition, Supervision, Writing – review & editing. **Heinz-Georg Jahnke:** Conceptualization, Data curation, Funding acquisition, Investigation, Methodology, Software, Supervision, Visualization, Writing – original draft, Writing – review & editing.

Declaration of competing interest

The authors declare that they have no known competing financial interests or personal relationships that could have appeared to influence the work reported in this paper.

Data availability

Data will be made available on request.

Acknowledgements

This work was funded by the European Union (EFRE) and the Saxon Ministry of Science and the Fine Arts (SMWK, project: “PhenoCor”, Grant No. 100387678/100387681 and “CardioEpix”, Grant No. 100685417/100685579) and is tax-supported on the basis of the budget approved by the members of the parliament of the Free State of Saxony. We thank Prof. Dr. William Claycomb for the provision of the HL-1 cell line.

Appendix A. Supplementary data

Supplementary data to this article can be found online at https://doi.org/10.1016/j.bios.2024.116120.

References

Azzolin, L., Schuler, S., Dossel, O., Loewe, A., 2021. Front. Physiol. 12, 656411.
Chang, M.G., Zhang, Y., Chang, C.Y., Xu, L., Emokpae, R., Tung, L., Marban, E., Abraham, M.R., 2009. Circ. Res. 105 (11), 1062–1071.
Claycomb, W.C., Lanson Jr., N.A., Stallworth, B.S., Egeland, D.B., Delcarpio, J.B., Bahinski, A., Izzo Jr., N.J., 1998. Proc. Natl. Acad. Sci. U. S. A. 95 (6), 2979–2984.
Cluitmans, M.J.M., Bayer, J., Bear, L.R., Ter Bekke, R.M.A., Heijman, J., Coronel, R., Volders, P.G.A., 2023. Front Cardiovasc Med 10, 1121517.
Cyganek, L., Tiburcy, M., Sekeres, K., Gerstenberg, K., Bohnenberger, H., Lenz, C., Henze, S., Stauske, M., Salinas, G., Zimmermann, W.H., Hasenfuss, G., Guan, K., 2018. JCI Insight 3 (12).
Emery, B.A., Hu, X., Khanzada, S., Kempermann, G., Amin, H., 2023. Biosens. Bioelectron. 237, 115471.
Feyen, D.A.M., McKeithan, W.L., Bruyneel, A.A.N., Spiering, S., Hormann, L., Ulmer, B., Zhang, H., Briganti, F., Schweizer, M., Hegyi, B., Liao, Z., Polonen, R.P., Ginsburg, K. S., Lam, C.K., Serrano, R., Wahlquist, C., Kreymerman, A., Vu, M., Amatya, P.L., Behrens, C.S., Ranjbarvaziri, S., Maas, R.G.C., Greenhaw, M., Bernstein, D., Wu, J.C., Bers, D.M., Eschenhagen, T., Metallo, C.M., Mercola, M., 2020. Cell Rep. 32 (3), 107925.
Fleischer, S., Jahnke, H.G., Fritsche, E., Girard, M., Robitzki, A.A., 2019. Biosens. Bioelectron. 126, 624–631.
Hasenfuss, G., Pieske, B., Castell, M., Kretschmann, B., Maier, L.S., Just, H., 1998. Circulation 98 (20), 2141–2147.
Hirt, M.N., Boeddinghaus, J., Mitchell, A., Schaaf, S., Bornchen, C., Muller, C., Schulz, H., Hubner, N., Stenzig, J., Stoehr, A., Neuber, C., Eder, A., Luther, P.K., Hansen, A., Eschenhagen, T., 2014. J. Mol. Cell. Cardiol. 74, 151–161.
Hu, N., Wang, T., Wan, H., Zhuang, L., Kettenhofen, R., Zhang, X., Zhang, Y.S., Xu, W., Gossmann, M., Bohlen, H., Hou, X., Wang, P., 2018. Biosens. Bioelectron. 117, 354–365.
Jahnke, H.G., Schmidt, S., Frank, R., Weigel, W., Pronnecke, C., Robitzki, A.A., 2019. Biosens. Bioelectron. 129, 208–215.
Kaheinen, P., Pollesello, P., Hertelendi, Z., Borbely, A., Szilagyi, S., Nissinen, E., Haikala, H., Papp, Z., 2006. Basic Clin. Pharmacol. Toxicol. 98 (1), 74–78.
Kovacs, M., Toth, J., Hetenyi, C., Malnasi-Csizmadia, A., Sellers, J.R., 2004. J. Biol. Chem. 279 (34), 35557–35563.
Kussauer, S., David, R., Lemcke, H., 2019. Cells 8 (11).
Limouze, J., Straight, A.F., Mitchison, T., Sellers, J.R., 2004. J. Muscle Res. Cell Motil. 25 (4–5), 337–341.
Miccoli, B., Lopez, C.M., Goikoetxea, E., Putzeys, J., Sekeri, M., Krylychkina, O., Chang, S.W., Firrincieli, A., Andrei, A., Reumers, V., Braeken, D., 2019. Front. Neurosci. 13, 641.
Nagy, L., Kovacs, A., Bodi, B., Pasztor, E.T., Fulop, G.A., Toth, A., Edes, I., Papp, Z., 2015. Br. J. Pharmacol. 172 (18), 4506–4518.
Pandit, S.V., Jalife, J., 2013. Circ. Res. 112 (5), 849–862.
Quiroga, R.Q., Nadasdy, Z., Ben-Shaul, Y., 2004. Neural Comput. 16 (8), 1661–1687.
Roney, C.H., Cantwell, C.D., Qureshi, N.A., Chowdhury, R.A., Dupont, E., Lim, P.B., Vigmond, E.J., Tweedy, J.H., Ng, F.S., Peters, N.S., 2017. Ann. Biomed. Eng. 45 (4), 910–923.
Schmidt, S., Frank, R., Krinke, D., Jahnke, H.G., Robitzki, A.A., 2022. Biosens. Bioelectron. 202, 114012.
Seidel, D., Jahnke, H.G., Englich, B., Girard, M., Robitzki, A.A., 2017. Analyst 142 (11), 1929–1937.
Shaheen, N., Shiti, A., Huber, I., Shinnawi, R., Arbel, G., Gepstein, A., Setter, N., Goldfracht, I., Gruber, A., Chorna, S.V., Gepstein, L., 2018. Stem Cell Rep. 10 (6), 1879–1894.
Shinnawi, R., Shaheen, N., Huber, I., Shiti, A., Arbel, G., Gepstein, A., Ballan, N., Setter, N., Tijsen, A.J., Borggrefe, M., Gepstein, L., 2019. J. Am. Coll. Cardiol. 73 (18), 2310–2324.
Stoppel, W.L., Kaplan, D.L., Black 3rd, L.D., 2016. Adv. Drug Deliv. Rev. 96, 135–155.
Tertoolen, L.G.J., Braam, S.R., van Meer, B.J., Passier, R., Mummery, C.L., 2018. Biochem. Biophys. Res. Commun. 497 (4), 1135–1141.
Tse, G., 2016. J Arrhythm 32 (2), 75–81.
Wang, T., Hu, N., Cao, J., Wu, J., Su, K., Wang, P., 2013. Biosens. Bioelectron. 49, 9–13.
Xu, L., Hu, C., Huang, Q., Jin, K., Zhao, P., Wang, D., Hou, W., Dong, L., Hu, S., Ma, H., 2021. Biosens. Bioelectron. 175, 112854.
Zhao, E.T., Hull, J.M., Mintz Hemed, N., Ulusan, H., Bartram, J., Zhang, A., Wang, P., Pham, A., Ronchi, S., Huguenard, J.R., Hierlemann, A., Melosh, N.A., 2023. Sci. Adv. 9 (23), eadf9524.